Si intralayers at GaAs/AlAs and GaAs/GaAs junctions: Polar versus nonpolar interfaces

M. Moreno*
Instituto de Ciencia de Materiales de Madrid (CSIC), Cantoblanco, E-28049 Madrid, Spain

H. Yang and M. Höricke
Paul-Drude-Institut für Festkörpelectronik, Hausvogteiplatz 5-7, D-10117 Berlin, Germany

M. Alonso and J. A. Martín-Gago
Instituto de Ciencia de Materiales de Madrid (CSIC), Cantoblanco, E-28049 Madrid, Spain

R. Hey
Paul-Drude-Institut für Festkörpelectronik, Hausvogteiplatz 5-7, D-10117 Berlin, Germany

K. Horn
Fritz-Haber-Institut der Max-Planck-Gesellshaft, Faradayweg 4-6, D-14195 Berlin, Germany

J. L. Sacedón
Instituto de Ciencia de Materiales de Madrid (CSIC), Cantoblanco, E-28049 Madrid, Spain

K. H. Ploog
Paul-Drude-Institut für Festkörpelectronik, Hausvogteiplatz 5-7, D-10117 Berlin, Germany
(Received 1 December 1997)

The effect of inserting thin Si intralayers at GaAs/AlAs and GaAs/GaAs interfaces has been studied by photoelectron spectroscopy (PES) using synchrotron radiation. Results from *polar* and *nonpolar* interfaces are compared by analyzing samples grown by molecular-beam epitaxy on (100) and (110) substrates, respectively. The Si intralayers were inserted by an improved δ-doping method in a concentration of $2.2\times 10^{14}\ \mathrm{cm}^{-2}$ [about $\frac{1}{3}$ of a (100) monolayer]. When Si is introduced at GaAs-on-AlAs interfaces, the Al($2p$)-to-Ga($3d$) energy distance is observed to increase for both polar and nonpolar interface orientations. The insertion of Si at GaAs/GaAs(110) homojunctions modifies the line shape of the Ga($3d$) and As($3d$) peaks, resembling the changes previously reported for the (100) orientation. The results on polar junctions previously obtained were generally interpreted as band-offset changes, which would be related according to the ''interface microscopic capacitor'' picture with the polar nature of the interface. The PES results here presented are difficult to reconcile with such a model because of the similar behavior shown by polar and nonpolar interfaces. Instead, they can be understood within an ''overlayer band bending'' interpretation. [S0163-1829(98)01519-7]

I. INTRODUCTION

At the interface between two semiconductors, the band-gap difference is shared between discontinuities in the valence and conduction bands. Understanding the mechanism of band alignment at the interface is important for both technological and fundamental reasons.[1,2] Device design requires a precise knowledge of the band offset, and the ability to control its value would mean an additional degree of freedom. From a fundamental point of view, an important issue has been to ascertain whether the band offset is determined by the bulk properties of the semiconductors composing the junction, or depends on the local interface properties.[3–11] Depending on the answer, the efforts devoted to control band offsets should be focused either on the selection of the junction components, or on the manipulation of the interface structure. The theoretical and experimental work performed up to now has not provided a generic answer.[12] While for some systems the band offset can be considered to be intrinsically fixed, for other systems its value can be controlled through interface structure manipulation. For instance, offsets of isovalent interfaces of the type IV/IV, or III-V/III-V and II-VI/II-VI with a common anion or cation (e.g., AlAs/GaAs) have been found to be independent of orientation and interface quality.[13–17] On polar (100) interfaces of isovalent compound junctions with no common anion (e.g., InAs/GaSb), the different interface configurations obtained by changing the interface terminating and initiating layers from each compound (i.e., InAs/GaSb and AsIn/SbGa) can show slightly different band-offset values, due to the modification of the interface dipole.[17,18] The group of AlAs-GaAs interfaces is one of the most thoroughly studied and best-characterized systems because of its abundant optoelectronic applications.[19,20] It belongs to the family of common-anion isovalent compound interfaces; therefore, the possibilities for changing the band offset are, in principle, limited. However, an ingenious idea has been proposed to modify it: i.e., the insertion of group-IV semiconductor intralayers.[21,22] The purpose is to convert an isovalent interface (III-V/III-V) into a double heterovalent one (III-V/IV+IV/III-V). At heterova-

0163-1829/98/57(19)/12314(10)/$15.00 © 1998 The American Physical Society

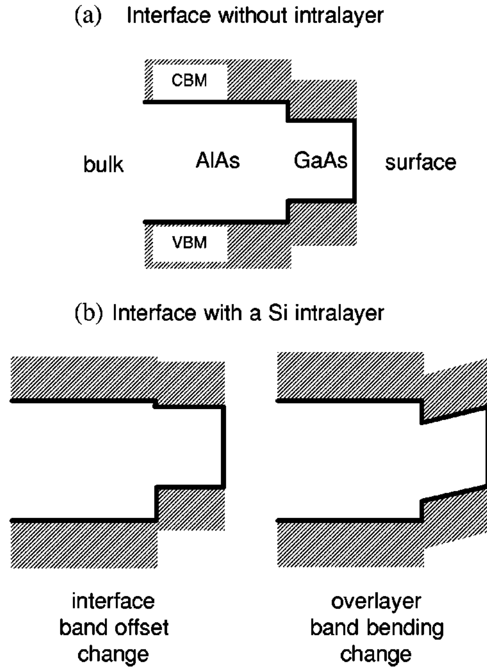

FIG. 1. Schematic band diagrams on GaAs-on-AlAs heterojunctions: (a) without intralayer, and (b) with a Si intralayer, according to the two competing models.

lent junctions (e.g., Si/GaAs), the offset seems to be determined by bulk properties on nonpolar interfaces, but it depends on the interface microscopic details for polar orientations.[23] Hence, a chance for band-offset modification arises on polar III-V/IV/III-V interfaces; nevertheless this possibility is expected to be restricted for nonpolar ones.

Theoretical calculations have predicted that the band offset of polar AlAs-GaAs(100) heterojunctions can be tuned by inserting group-IV atoms (Si or Ge) at the interface.[22] On GaAs-GaAs(100) homojunctions, it has also been predicted that the insertion of group-IV atoms can induce a band offset.[21] Using photoelectron spectroscopy (PES), Sorba *et al.*[24] studied the effect of Si intralayers at AlAs-GaAs(100) heterojunctions, and Marsi *et al.*[25] at GaAs-GaAs(100) homojunctions. Their PES results were interpreted as a demonstration of the band-offset tuning effect theoretically predicted. However, some criticisms of this interpretation have argued that the PES results obtained on AlAs-GaAs heterojunctions could be connected with the existence of a sharp overlayer band bending rather than with a real modification of the band offset.[26,27] The band diagrams for the two competing models are depicted schematically in Fig. 1. Thus the viability on these systems of the band-offset control by intralayer insertion is still a matter of debate, which needs further verification even for the case of polar interfaces.

Results from linear-response theory indicated that band-offset modification is not possible at nonpolar interfaces.[23] The first-principles calculations of Christensen and Brey confirmed that at AlAs-GaAs(110) interfaces, the insertion of interlayers has little or no effect on the band offsets.[28] In contrast, the calculations of Muñoz and Rodríguez-Hernández predicted a significant tuning effect for insertion of Si or Ge at AlAs-GaAs(110) interfaces.[29] However, in the latter work the tuning effect seems to be a result of the specific type of sites chosen in the calculations for the intralayer atoms, rather than a consequence of the nonpolar geometry of the interface. From an experimental point of view, investigations of intralayer insertion at nonpolar III-V/III-V junctions are very scarce. The maturity of the molecular-beam-epitaxy (MBE) growth technique on the [100] orientation has favored the study of polar interfaces. Growth on the nonpolar [110] orientation is more difficult;[30,31] however, the state of the art of the (110) growth has lately reached an acceptable quality level.[32–35] To our knowledge, the work of Ref. 27 is the only PES result existent for nonpolar junctions of this type.[27] This group reported the value of the *apparent* band offset at Si-containing AlAs-on-GaAs(110) heterojunctions, as compared with other (100) and (311) interface orientations.[27]

Most previous studies have used conventional x-ray photoelectron spectroscopy (XPS); however, synchrotron radiation sources are more convenient because they provide a better energy resolution and a higher photon flux. In this paper we use core-level and valence-band PES with synchrotron radiation to investigate the effect of submonolayer Si insertion at GaAs-on-AlAs(100) and (110) heterojunctions, and at GaAs-GaAs(110) homojunctions. We examine the influence of the interface polarity nature on the *apparent* band offset. Our experimental results are discussed within the framework of the different models proposed to explain previous data on polar interfaces. A qualitatively different behavior is expected for polar and nonpolar interfaces within the ''interface microscopic capacitor'' model used to predict the band-offset tuning effect, while within an ''overlayer band-bending'' interpretation a certain insensitivity to the interface polarity can be understood. Therefore, the conclusions of our comparative study of polar and nonpolar interfaces may help to clarify the present controversy existent in the field.

II. EXPERIMENT

The GaAs/AlAs heterojunctions and the GaAs/GaAs homojunctions of the present study were grown by MBE on differently oriented substrates. We used epiready heavily Si doped ($n=1\times10^{18}$ cm^{-3}), (100)-2° off toward (111)A, and (110)-oriented, GaAs substrates. A (0.1–0.3)-μm-thick Si-doped ($n=1\times10^{18}$ cm^{-3}) GaAs buffer layer was first grown, followed by a 200-Å-thick undoped AlAs (or GaAs) layer. At this point a layer of Si, with a density of 2.2×10^{14} cm^{-2}, was inserted in some samples. Finally, all samples were terminated by a 20-Å-thick nominally undoped GaAs layer.

The main problems that the growth of this kind of structures encounters are (i) faceting when growing on (110)-oriented substrates, and (ii) surface segregation of Si. The growth methods that we used attempted to minimize such difficulties. Growth parameters are summarized in Table I. Growth rates were calibrated by means of reflection high-energy electron-diffraction specular-beam intensity oscillations. Si flux was determined by capacitance-voltage profiling measurements on homogeneously n-doped GaAs calibration layers. The substrate temperature during growth was measured using a thermocouple, placed at the back of the substrate holder, which was calibrated by taking as a reference point the temperature of the GaAs oxide desorption

TABLE I. MBE-growth parameters of the different types of samples analyzed here.

	GaAs/AlAs(100)	GaAs/Si/AlAs(100)	GaAs/AlAs(110)	GaAs/Si/AlAs(110)	GaAs/GaAs(110)	GaAs/Si/GaAs(110)
Substrate						
orientation	(100)-2°→(111)*A*	(100)-2°→(111)*A*	(110)	(110)	(110)	(110)
Si doping	1×10^{18} cm^{-3}	1×10^{18} cm^{-3}	1×10^{18} cm^{-3}	1×10^{18} cm^{-3}	1×10^{18} cm^{-3}	1×10^{18} cm^{-3}
Buffer layer						
thickness	0.3 μm	0.3 μm	0.1 μm	0.1 μm	0.06 μm	0.06 μm
T (substrate)	590 °C	590 °C	485 °C	485 °C	455 °C	455 °C
growth rate	0.44 μm/h	0.44 μm/h	0.16 μm/h	0.16 μm/h	0.19 μm/h	0.19 μm/h
Si doping	1×10^{18} cm^{-3}	1×10^{18} cm^{-3}	1×10^{18} cm^{-3}	1×10^{18} cm^{-3}	1×10^{18} cm^{-3}	1×10^{18} cm^{-3}
Buried layer						
thickness	200 Å (AlAs)	200 Å (AlAs)	200 Å (AlAs)	200 Å (AlAs)	200 Å (GaAs)	200 Å (GaAs)
T(substrate)	610 °C	610 °C	505 °C	505 °C	485 °C	485 °C
growth rate	0.36 μm/h	0.36 μm/h	0.18 μm/h	0.18 μm/h	0.19 μm/h	0.19 μm/h
Si doping						
Si intralayer						
2D density		2.2×10^{14} cm^{-2}		2.2×10^{14} cm^{-2}		2.2×10^{14} cm^{-2}
T (substrate)		590 °C		505 °C		485 °C
flux (pulsed)		2×10^{11} cm^{-2} s^{-1}		2×10^{11} cm^{-2} s^{-1}		2×10^{11} cm^{-2} s^{-1}
Overlayer (GaAs)						
thickness	20 Å	20 Å	20 Å	20 Å	20 Å	20 Å
T (substrate)	590 °C	540 °C	505 °C	385-485 °C	485 °C	385-485 °C
growth rate	0.44 μm/h	0.44 μm/h	0.16 μm/h	0.16 μm/h	0.19 μm/h	0.19 μm/h
Si doping						

[580 °C on (100) GaAs]. The growth on (100) GaAs was performed under standard conditions. However, if the growth on (110) GaAs takes place under these ''standard (100) conditions,'' faceting occurs, due to the preferred formation of triangular-shaped islands.[30,31] Therefore, the conditions for growth on (110) GaAs were carefully optimized to guarantee a smooth surface morphology. The optimization procedure included atomic force microscopy (AFM) characterization to select the appropriate substrate temperatures, As flux, and growth rates.[34] Si insertion was performed following an improved δ-doping protocol, which is different from the method used on previous PES studies. We employed a *pulsed low-flux* Si deposition technique and a slight misorientation [2° off toward (111)*A*] in (100)-oriented structures to improve the structural quality of the inserted Si layer.[36] The growth of the GaAs overlayer in samples containing a Si intralayer was performed at a reduced substrate temperature, to minimize the possibility of Si segregation.

The samples were vacuum-transferred after the MBE growth to a carousel inside a small UHV chamber with a base pressure in the high-10^{-10}-mbar range. This chamber was carried to the synchrotron facility BESSY I (Berliner Elektronenspeicherring-Gesellschaft für Synchrotronstrahlung mbh I), where the samples were again vacuum-transferred to the photoemission analysis chamber, which was connected to the TGM2 or TGM6 beam lines. PES measurements were performed no later than one week after the MBE growth. We used a multiple sample holder which accommodated several samples, such that these could be consecutively measured under the same experimental conditions. The samples and a gold foil were placed together in the analysis chamber under electrical contact, and grounded. We used a heavily doped substrate to prevent the samples from being charged during the photoemission analysis. Electron kinetic-energy distribution curves (EDC's) were recorded for each sample. Electrons were collected and counted in the normal emission geometry by an angle-resolving analyzer. The Ga($3d$), Al($2p$), and As($3d$) core-level and valence-band-edge emissions from each sample, as well as the Fermi-edge emission from the gold foil, were consecutively recorded at a fixed photon energy. This procedure was repeated for several photon energies. The overall energy resolution was 150–300 meV in the range of photon energies used (40–95 eV).

III. RESULTS AND DISCUSSION

A. Heterojunctions

Determining the band discontinuity at the interface between two semiconductors A and B by core-level photoemission spectroscopy involves the measurement of the energy separation, $\Delta E_{\rm CL}$, between two core levels corresponding to each side of the interface.[37–39] The valence-band offset ΔE_V is directly determined by subtracting a quantity ξ that accounts for the energy difference between the respective core-level binding energies,

$$\Delta E_V = \Delta E_{\rm CL} - \xi \qquad (1)$$

where

$$\Delta E_V = E_V^B - E_V^A,$$

$$\Delta E_{\rm CL} = E_{\rm CL}^B - E_{\rm CL}^A,$$

$$\xi = (E_{\rm CL}^B - E_V^B) - (E_{\rm CL}^A - E_V^A).$$

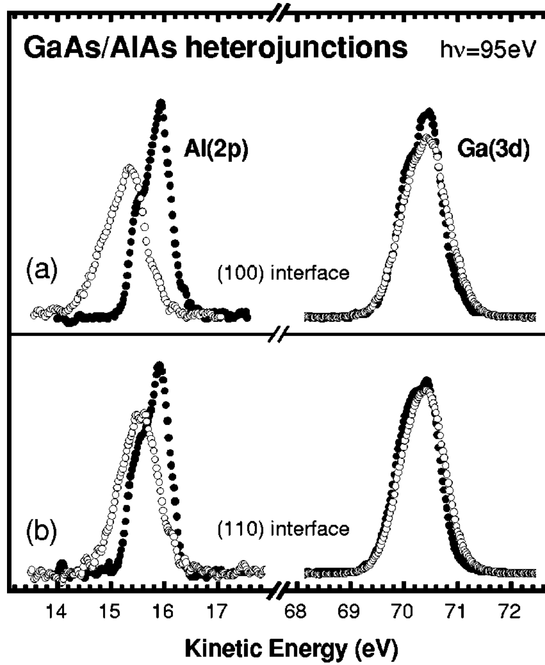

FIG. 2. Al($2p$) and Ga($3d$) core-level spectra recorded on GaAs/AlAs (solid circles) and GaAs/Si/AlAs (open circles) heterojunctions (GaAs on top), using 95-eV photons. Results for (a) (100)-, and (b) (110)-oriented interfaces. The concentration of the Si intralayer is 2.2×10^{14} cm^{-2}, which corresponds to $\frac{1}{3}$ of a (100) monolayer, or equivalently to $\frac{1}{4}$ of a (110) monolayer. The spectra are shown after peak-area normalization.

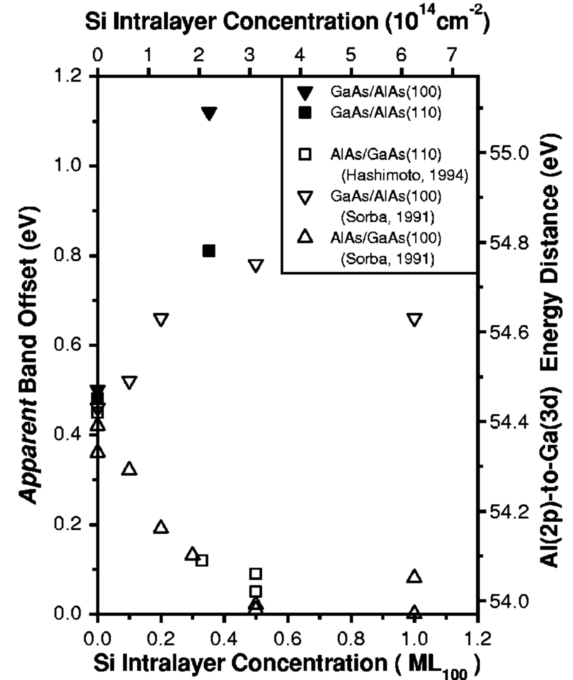

FIG. 3. *Apparent* band offset and related Al($2p$)-to-Ga($3d$) energy distance of AlAs-Si-GaAs interfaces determined by core-level PES for different orientations and stacking sequences. Our results (solid symbols) and those reported by other groups (open symbols) are shown as a function of the nominal Si-intralayer concentration.

This method is very simple; however, it is accurate only if certain conditions are fulfilled: the energy levels along the photoemission probing depth must be well-defined levels. If chemical reactions or band-bending effects are present, the analysis should be made very carefully, since these effects may broaden and/or shift the recorded core-level peaks, and lead to inaccuracy.

Figure 2 shows Al($2p$) and Ga($3d$) EDC spectra obtained when irradiating GaAs-on-AlAs heterostructures with 95-eV photons. Results from samples without (solid symbols) and with (open symbols) a Si intralayer are compared, for the (100) [Fig. 2(a)] and (110) [Fig. 2(b)] interface orientations. The concentration of the Si intralayer is 2.2×10^{14} cm^{-2}. This two-dimensional concentration corresponds to approximately $\frac{1}{3}$ of the atomic sites in a (100) monolayer, and to $\frac{1}{4}$ of the atomic sites in a (110) monolayer, or equivalently to $\frac{1}{2}$ of the Ga sites in a (110) monolayer. The spectra are shown without performing any kind of energy scale alignment. The intensities of the core-level spectra displayed have been area normalized, that is, the peaks that are compared have the same area. The kinetic-energy scale is the same for all of the samples, since these were kept under electrical contact and were measured consecutively under the same experimental conditions. Upon Si insertion, the Ga($3d$) peak—from the GaAs overlayer—remains at nearly the same position, while the Al($2p$) peak—from the AlAs buried layer—shifts toward lower kinetic energies. Thus an increase of the Al($2p$)-to-Ga($3d$) energy distance is observed on Si-containing heterostructures relative to those without an intralayer. Remarkably, this effect is observed on *both* polar (100) and nonpolar (110) interfaces, although it is smaller on the (110) interface.

The valence-band offset can be obtained from the measured core-level offset, ΔE_{CL}, using Eq. (1), with a value for ξ of 54.00 eV [derived from the known binding energies, 72.86 and 18.86 eV, for the Al($2p$) and Ga($3d$) core levels in AlAs and GaAs, respectively].[24] The core-level offset has been obtained from the energy difference between the respective centroids, where ''centroid'' is defined as the energy value that divide the core-level peak into two parts of equal area. The band-offset values determined in such a manner, ΔE_V^*, will be called in what follows *apparent* band offsets. They correspond to the *real* band offsets only if the energy values derived from the experimental core-level data actually correspond to the *interface* values. Flatband conditions, the absence of chemical reactions, and the employment of experimental conditions as bulk sensitive as possible allow us to satisfy the above premise.

The Al($2p$)-to-Ga($3d$) core-level energy distances obtained for the clean interfaces are 54.50 and 54.48 eV, for the (100) and (110) orientations, respectively. Hence, the *apparent* valence-band offsets are 0.50 and 0.48 eV, respectively. That is, as expected for isovalent compound interfaces with common anion, the offset is within error margin independent of interface orientation. The core-level energy distance measured on (100) Si-containing heterostructures is 55.12 eV, giving an *apparent* valence-band offset of 1.12 eV; thus ΔE_V^* increases by 0.62 eV relative to the offset on heterostructures without an intralayer. On GaAs/Si/AlAs(110) structures, the core-level distance is 54.81 eV; the *apparent* valence-band offset is thus 0.81 eV, that is 0.33 eV larger than the offset in GaAs/AlAs(110) junctions.

Figure 3 shows the comparison of the present results

(solid symbols) with the previously reported ones for the AlAs-GaAs system (open symbols). The *apparent* valence-band offset that we have obtained for Si-containing (100) interfaces (1.12 eV) is markedly higher than the value previously reported for the same nominal Si concentration (0.65 eV for $\frac{1}{3}$ ML).[24] Both results are not directly comparable because of the different Si-deposition method employed (pulsed low-flux versus continuous deposition); however, it is noticeable that the value obtained here for $\frac{1}{3}$ ML of Si (1.12 eV) is even higher than the saturation value previously reported (0.78 eV), which was obtained for a Si concentration of $\frac{1}{2}$ ML.[24] Our results for GaAs-on-AlAs(110) [Fig. 2(b)], together with the data reported for AlAs-on-GaAs(110),[27] indicate that, for nonpolar interfaces, there is an *increase* or *decrease* of the apparent valence-band offset depending on the stacking sequence, similarly to what was found for polar interfaces.[24] Muñoz and Rodríguez-Hernández predicted a *reduction* of the valence-band offset at Si-containing AlAs-GaAs(110) interfaces relative to the offset on interfaces without intralayer.[29] Experimentally, we obtain an *increase* of the apparent offset at GaAs-on-AlAs(110) interfaces containing $\frac{1}{4}$ ML of Si. In our opinion, both results should not be directly compared because the above theoretical calculation refers to structural conditions very ideal and quite different from the ones that can be achieved in practice, and especially because this calculation does not include the presence of the surface. Note that for the (110) orientation the stacking sequence has no meaning within this type of calculation, contrary to the clear qualitative influence that is observed experimentally (Fig. 3).

Essentially, our experimental results show that the effect of Si insertion, as examined by photoemission spectroscopy, is quite similar for polar (100) and nonpolar (110) interfaces (Fig. 2). Si insertion at GaAs-AlAs heterointerfaces produces large changes of the Al($2p$)-to-Ga($3d$) energy separation measured by PES. However, can these changes be correctly evaluated as band-offset changes? Let us first analyze, from a theoretical point of view, how the intralayer may act to induce a band-offset change. Two mechanisms have been proposed to be involved. One is the establishment of charged interfaces of opposite polarity, of the so-called *interface microscopic capacitor*. As explained above, a III-V/III-V isovalent interface with a group-IV intralayer can be viewed as a pair of III-V/IV heterovalent interfaces. Polar interfaces between heterovalent semiconductors, if ideally abrupt, should be charged. The situation is thermodynamically unstable but, if the intralayer is thin enough, the increase in the free energy of the system is small and the two heterovalent III-V/IV interfaces may remain charged,[40] and may act as the parallel plates of a microscopic capacitor.[41] The positively (negatively) charged interface would correspond to the side where the material is anion (cation) terminated [Fig. 4(a)]. The establishment of this type of microscopic capacitor produces a potential drop at the interface, thus changing the band offset. A second mechanism leads to the formation of *neutral nonequivalent interfaces*.[12] Reduction of the free energy of the system and neutrality are achieved through formation of point defects and atomic mixing.[41,42] Multiple interface configurations result from this atomic mixing, thus producing different band discontinuity values.[43,44]

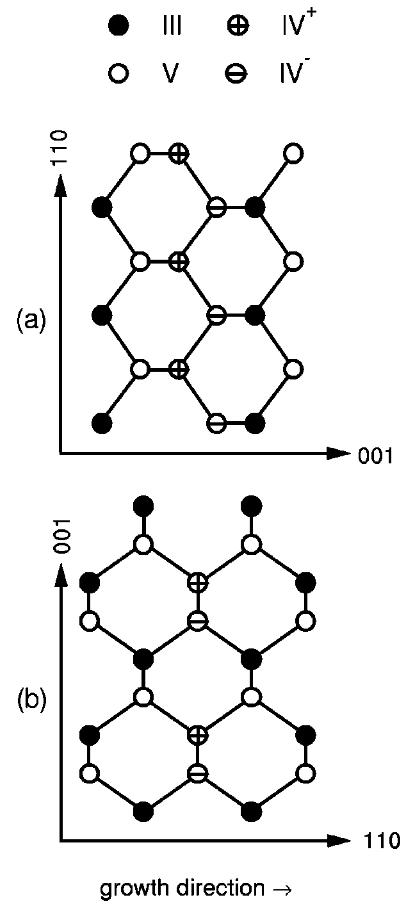

FIG. 4. Schematic representation of the charge transfer expected at (a) (100)-polar, and (b) (110)-nonpolar III-V/IV/III-V interfaces according to the Harrison's ''interface microscopic capacitor'' picture.

Within the interface microscopic capacitor picture, the *polar* character of the interface, considered from a geometric point of view, plays a key role in the modification of the band offset. A polar geometry would induce a charge transfer *crossing* the interface [Fig. 4(a)]. Conversely, at nonpolar junctions the charge transfer would take place *along* and not *across* the interface [Fig. 4(b)]; thus the interface—if layer averaged—would not be charged. Therefore, according to the microscopic capacitor model, band-offset changes are expected to occur on polar interfaces but not on nonpolar ones. Note that these arguments are valid for heterojunctions and homojunctions. Our experimental findings can hardly be reconciled with this model. If the experimental core-level shifts observed are interpreted as band-offset changes, this would mean that such changes take place on both polar and nonpolar interfaces. It would also mean that on both orientations it is possible to produce an increase or a decrease of the valence-band offset, simply by selecting the appropriate GaAs-on-AlAs or AlAs-on-GaAs stacking sequence, respectively. Pure *geometric* arguments cannot explain why the band offset should change at nonpolar interfaces. Perhaps the *chemical asymmetry* existing between each side of the interface could account for a Si-induced dipole *crossing* a nonpolar interface. If this explanation actually holds, the same increase or decrease of the band offset should take place at the nonpolar interface, independently of the stacking se-

quence. However, this is not the behavior observed experimentally; on the contrary, an *increase* or *decrease* of the apparent band offset is found, depending on the stacking sequence considered. Thus the interpretation of the experimental results as band-offset changes seems inconsistent with the interface microscopic capacitor model. A model based on the establishment of ''neutral nonequivalent interfaces'' could probably account for band-offset changes on nonpolar interfaces. Actually, for any experimental result, one could likely find a suitable configuration giving rise to a theoretical offset in agreement with experiment.[12] However—as Franciosi and Van de Walle noted—''this is no guarantee that the selected configuration is appropriate to describe the actual interface.''[12]

Our results can be readily understood within an ''overlayer band bending'' interpretation,[26,27] without including band offset changes, as follows. The n-type doping character of the Si intralayer induces a sharp upward overlayer band bending. This bending is then reflected in an increase (decrease) of the Al($2p$)-to-Ga($3d$) energy distance measured by PES on GaAs-on-AlAs (AlAs-on-GaAs) heterostructures, *independently* of the polarity nature of the interface.

B. Homojunctions

In homojunctions, the investigation of interface properties by photoemission is more difficult than in the case of heterojunctions. PES is an averaging technique that ''looks'' through the surface. When studying heterojunctions, the signals coming from the overlayer and the buried layers can be chemically discriminated by looking at two different core levels, characteristic of each side of the interface. In homojunctions, one is forced to separate both signals by deconvolving a single core-level line which contains information from both sides of the interface. The high resolution and the ability to vary the bulk sensitivity that synchrotron radiation sources provide are indispensable in this respect for the study of homojunctions. Figure 5 shows the As($3d$), Ga($3d$), and valence-band-edge EDC spectra from GaAs/GaAs(110) homojunctions without intralayer (solid symbols) and with a Si intralayer (open symbols), obtained with different photon energies. The corresponding reference Fermi-edge spectra from the gold plate are also shown. For each photon energy, spectra were recorded consecutively on both samples, under the same experimental conditions. Core-level spectra are shown after peak area normalization. The original kinetic-energy scale was translated into a binding-energy scale, whose energy zero was arbitrarily chosen at the energy position of the bulk Ga($3d_{5/2}$) component from pure GaAs(110). This energy position was obtained from the fitting of the Ga($3d$) spectra recorded from pure GaAs(110), to be shown below. In order to discriminate the shifts induced by a variation of the Fermi level pinning position at surface (E_F^{surf}), and those shifts with a different origin, the whole set of spectra from the Si-containing homojunction was rigidly shifted until the valence-band edges from the samples with and without Si intralayer were coincident. The ''apparent'' shift of the Fermi edge, displayed in Fig. 5, originates on the above alignment procedure. This shift simply means a change of the Fermi-level surface pinning position, which is consistently reproduced at the three photon energies used. Upon Si

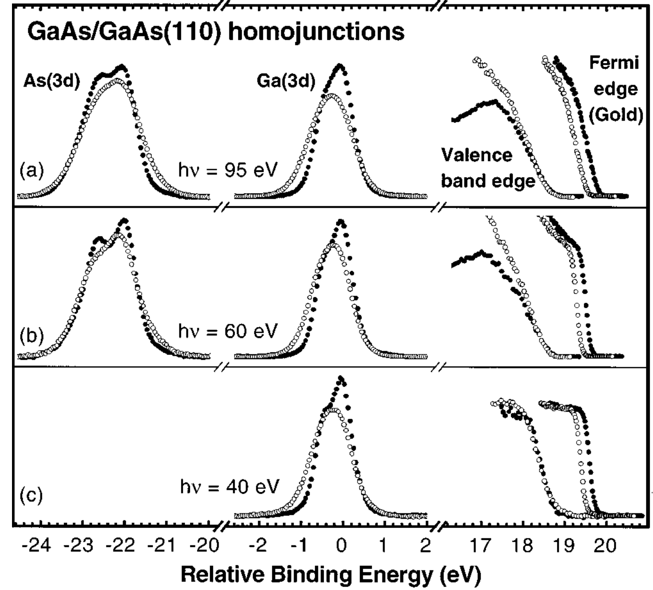

FIG. 5. As($3d$), Ga($3d$), and valence-band-edge EDC spectra obtained by illuminating GaAs(110) (solid circles) and GaAs/Si/GaAs(110) (open circles) samples with (a) 95-eV, (b) 60-eV, and (c) 40-eV photons. Gold Fermi-edge spectra are also displayed for reference. The set of spectra from Si-containing homojunctions has been rigidly shifted until the valence-band edges from the samples with and without a Si intralayer were coincident. Core-level spectra are shown after peak-area normalization.

insertion, the Fermi level approaches the valence-band maximum at surface. In pure GaAs(110), E_F^{surf} lies 0.5 eV below E_C, while in GaAs/Si/GaAs(110) it lies 0.7 eV below E_C. Variation of the bulk sensitivity, within the photon energy range considered (40–95 eV), does not significantly modify the core-level line shapes from both samples. The slight changes observed are mainly due to the improvement on the monochromator resolution when the photon energy decreases. Upon Si insertion, the Ga($3d$) and As($3d$) emissions clearly broaden. On the Ga($3d$) peak a substantial part of the emission is transferred toward the high-binding-energy side, while on the As($3d$) peak an appreciable transfer takes place toward lower binding energies.

A detailed core-level line-shape analysis has been performed in order to obtain further information. The experimental curves were fitted as summations of several Voigt spin-orbit-split doublets, using a least-squares minimization routine based on the Levenberg and Marquardt algorithm. Figure 6 shows line-shape analysis of As($3d$) and Ga($3d$) spectra recorded on GaAs/GaAs(110) homojunctions, without and with a Si intralayer, using 60-eV photons. The spectra selected for the line-shape analysis correspond to different surface sensitivity conditions; however, the parallel analysis of the core-level emissions recorded at a fixed photon energy allows us to determine accurately the energy separation between the As($3d$) and Ga($3d$) bulk components. The line-shape analysis started on the spectra taken on pure GaAs(110). To our knowledge, these are the first EDC spectra reported for *MBE-prepared* GaAs(110) surfaces. The line-shape analysis showed that the spectra recorded on our MBE-prepared GaAs(110) surfaces cannot be explained using the same type of components as the typically reported for GaAs(110) surfaces obtained by *cleaving* in UHV.[45,46] Table

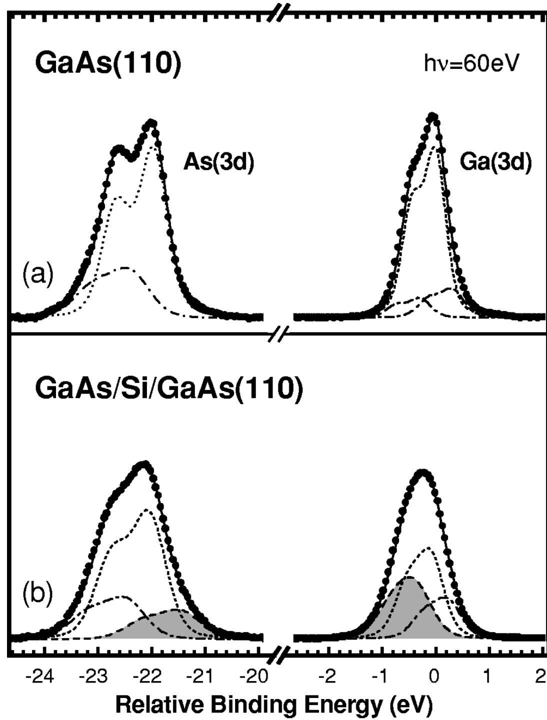

FIG. 6. Results from the line-shape analysis of As(3*d*) and Ga(3*d*) spectra recorded on as-MBE-grown (a) GaAs(110), and (b) GaAs/Si/GaAs(110) samples, using 60-eV photons. Besides the experimental data points (solid symbols), the fit curve (solid line) and the corresponding components are also shown. The dotted lines refer to the bulk emissions; the shaded areas correspond to Si-induced contributions.

II summarizes the main line-fitting parameters. Two components are enough to fit the As(3*d*) peak; the doublet with the lower intensity appears shifted toward higher binding energies. In order to fit the Ga(3*d*) peak, three doublets are needed, with two small components on either side of a main signal. Curiously, this kind of deconvolution scheme resembles more the ''three-components fit'' usually performed for MBE-prepared GaAs(100) surfaces,[47,48] than the ''two-components fit'' of the typical Ga(3*d*) spectra recorded on cleaved GaAs(110) samples.[45,46] At the moment we cannot offer a conclusive explanation of this result. The main doublets (dotted lines) probably reflect bulk emissions. The peak-shape similarities between the Ga(3*d*) spectra from our MBE-prepared GaAs(110) surfaces, and those previously reported for MBE-prepared GaAs(100) surfaces, suggest that the low-intensity components (dash-dotted lines) may have a common origin on both orientations, connected with the special features of the MBE surface preparation method. The anomalous line shape of the Ga(3*d*) spectra recorded on our GaAs(110) samples could also be a manifestation of the existence of lateral variations in the surface barrier height.[49,50]

TABLE II. Fitting parameters resulting from the line-shape analysis of Ga(3*d*) and As(3*d*) core-level spectra recorded on as-MBE-grown GaAs(110) surfaces using 60-eV photons.

Parameter	Ga(3*d*)	As(3*d*)
Spin-orbit splitting	0.44	0.70
Branching ratio	1.5	1.5
Lorentzian FWHM	0.15	0.17
Gaussian FWHM *B*	0.37	0.53
Gaussian FWHM *S*1	0.37	0.76
Gaussian FWHM *S*2	0.41	
Binding energy *B*	0.00	−21.96
BE shift *S*1	+0.28	+0.44
BE shift *S*2	−0.32	

In order to fit the core-level spectra from GaAs/Si/GaAs(110), shown in Fig. 6(b), we used as a basis the results obtained for pure GaAs(110) (Table II). We employed the same type of components, but variations of the relative intensities and additional broadenings were allowed. When necessary, new doublets were introduced, trying always to use the smallest number of components. To maintain the consistency of the fit, the As($3d_{5/2}$)-to-Ga($3d_{5/2}$) energy distance between the main ''bulk'' components from GaAs/Si/GaAs(110) was kept fixed on the same value as the one obtained for pure GaAs(110). In order to achieve a reasonable fit of the As(3*d*) peak, an additional doublet had to be introduced, shifted by 0.48 eV toward the low-binding-energy side [the shaded area in Fig. 6(b)]. As for pure GaAs(110), the Ga(3*d*) peak from GaAs/Si/GaAs(110) can be explained simply with three doublets, but it is necessary to allow a larger shift (0.45 eV) of the high-binding-energy component [the shaded area in Fig. 6(b)]. A significant part of the Ga(3*d*) bulk signal on pure GaAs(110) seems to have been transferred to this component on GaAs/Si/GaAs(110) homojunctions. At this stage it is difficult to give a firm interpretation of the results of the above line-shape analysis. The line fits displayed in Fig. 6 are not intended to be ''conclusive'' ones. With them we are just trying to show up the main shape differences between the spectra taken on samples with and without a Si intralayer. There are effects, likely thought to occur on Si-containing structures, which have not yet been introduced in the discussion, and which could cause the apparition of additional spectral components. Segregation of Si is known to occur to some extent. Irrespective of whether Si atoms remain localized at the interface or segregate out, Si insertion induces a structural disorder because of its 4% lattice mismatch with GaAs. Chemically shifted components may appear as a result of the different chemical environment surrounding those As and Ga atoms located in the vicinity of Si atoms.

If Si insertion were to induce a band discontinuity in our (110) homojunctions, as Marsi *et al.* reported for (100) homojunctions,[25] one would expect to detect signals of this effect in the core-level spectra recorded with photon energies providing high enough bulk sensitivity, since these spectra should contain significant contributions from both the overlayer and the buried layer. The experimental data obtained for GaAs/Si/GaAs(110) do not lend themselves to such an interpretation, first, because variation of the bulk sensitivity does not significantly modify the core-level line shapes (Fig. 5), and second, because the extra emissions found for Si-containing structures are shifted in *opposite* directions for the As(3*d*) and Ga(3*d*) peaks [shaded areas in Fig. 6(b)], contrary to what one should observe if these shifts were to be caused by a band-offset modification. Nevertheless, the As(3*d*) and Ga(3*d*) spectra taken on our GaAs/Si/GaAs(110)

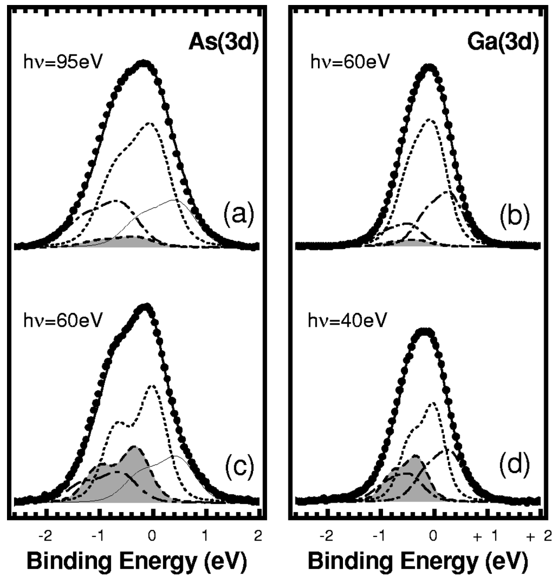

FIG. 7. Line fitting of As(3*d*) and Ga(3*d*) core-level spectra taken on GaAs/Si/GaAs(110) in (a) and (b) surface-sensitive conditions, and (c) and (d) bulk-sensitive conditions. The deconvolution model here considered distinguishes two bulk contributions: (i) the emission originated within the overlayer (dotted line), and (ii) the emission originated within the buried layer (shaded area). The meaning of the remaining components shown is the same than in Fig. 6(a), except the solid line in (a) and (c), which corresponds to a Si-induced feature.

samples (open symbols in Fig. 5) are not very different from those reported by Marsi *et al.* for the (100) orientation.[25] In fact, one can ''force'' an interpretation of the core-level line shapes in the same terms than those found in the scheme followed by Marsi *et al.* This is illustrated in Fig. 7 for data taken using different photon energies. Surface-sensitive conditions for the As(3*d*) and Ga(3*d*) core-level emissions are obtained when irradiating the sample with 95- and 60-eV photons, respectively (Figs. 7(a) and 7(b)]. Under these conditions, one can find a reasonably good fit where only the bulk component originating in the overlayer side of the structure is significant. More bulk-sensitive conditions are obtained when the As(3*d*) emission is recorded with 60-eV photons [Fig. 7(c)], and the Ga(3*d*) emission with 40-eV photons [Fig. 7(d)]. A second bulk component coming from the buried layer may be found in the corresponding spectra [shaded areas in Figs. 7(c) and 7(d)]. Besides the bulk signals, the line fits shown in Fig. 7 include other additional contributions. The two extra components of the Ga(3*d*) peaks, and the doublet shifted toward the high-binding-energy side of the As(3*d*) spectra (dash-dotted lines in Fig. 7) have the same meaning as the corresponding doublets found on pure GaAs(110) [dash-dotted lines in Fig. 6(a)]. However, the doublet found at the low-binding-energy side on the As(3*d*) peak from GaAs/Si/GaAs(110) [thin solid lines in Figs. 7(a) and 7(c)] did not exist on pure GaAs(110), and should rather be considered a Si-induced feature. The As(3*d*) and Ga(3*d*) buried-layer bulk components are both shifted relative to the respective overlayer bulk signals by 0.32 eV toward higher binding energy. Similar relative shifts found by Marsi *et al.* on (100)-oriented GaAs/Si/GaAs homojunctions were explained as a manifestation of the band offset induced at the homointerfaces by the Si insertion.[25] In principle, our experimental data could be interpreted in the same way. This would mean that Si insertion also induces a band offset at nonpolar interfaces.

The line-shape analysis scheme shown in Fig. 7, although possible, is not unique. Our data on the (110) orientation can be also explained without assuming that a band offset is induced by the Si insertion. Since the As(3*d*) and Ga(3*d*) spectra from Si-containing (110) homojunctions can be explained using three components [Fig. 6(b)], it is easy to understand that a good fit can be also achieved by introducing additional components in the analysis. Therefore, the line-shape analysis scheme shown in Fig. 7 seems somehow artificial. The experimental raw data show little evidence of a peak shape variation when varying the bulk sensitivity, and this provides a weak justification for the introduction of extra components. A second worrying aspect is that a good fit in Fig. 7 can only be obtained if the As($3d_{5/2}$)-to-Ga($3d_{5/2}$) energy distance between the bulk components is set as a variable parameter, resulting in a value that differs by 0.1 eV from the distance determined for pure GaAs(110) (Table II).

A different effect that may be present in our Si-containing homojunctions is the existence of a sharp band bending along the overlayer region. This effect was already considered in Sec. III A, for heterojunctions, and it is thought likely also to exist in homojunctions. In our GaAs/Si/GaAs(110) structures, the surface Fermi level has been experimentally determined to be located 0.7 eV below E_C (Fig. 5). Because of the heavy n-type substrate doping, the Fermi level in the bulk lies close to the conduction-band minimum. The difference between the E_F positions at the surface and in the bulk, relative to E_C, informs us that the total band bending across the entire GaAs/Si/GaAs semiconductor structure amounts 0.7 eV. Let us assume a model situation in which this 0.7-eV bending is confined within the overlayer region, as depicted in the inset of Fig. 8 (solid lines). This situation would be somehow justified by the extremely high n-type doping concentration provided by the Si intralayer, which certainly must induce a significant shortening of the Debye length that characterizes the extension of the surface depletion region. Figure 8 illustrates how the type of band bending assumed above could affect the shape of the As(3*d*) and Ga(3*d*) emissions experimentally recorded. PES spectra are the result of the summation of the different monolayer emissions, progressively attenuated for increasing depths because of photoelectron scattering. Such attenuation is governed by an exponential law which depends on the electron escape depth λ. If the bands are bent in the near-surface region, each monolayer contribution will be energy shifted by a certain amount according to the band profile. Figure 8(a) compares the Ga(3*d*) and As(3*d*) *bulk* emissions for homojunctions with *flat* overlayer bands and with *sharply bent* bands. The dashed curves in Fig. 8(a) correspond to the *bulk* components extracted from the line-shape analysis of the core levels recorded on pure GaAs(110) [Fig. 6(a)], whose bands were assumed to be flat along the photoemission probing depth. The thick solid lines in Fig. 8(a) display the line shapes calculated for the *band-bent* profile assumed above, and the thin solid lines represent the corresponding monolayer contributions. The typical photoelectron escape-depth values re-

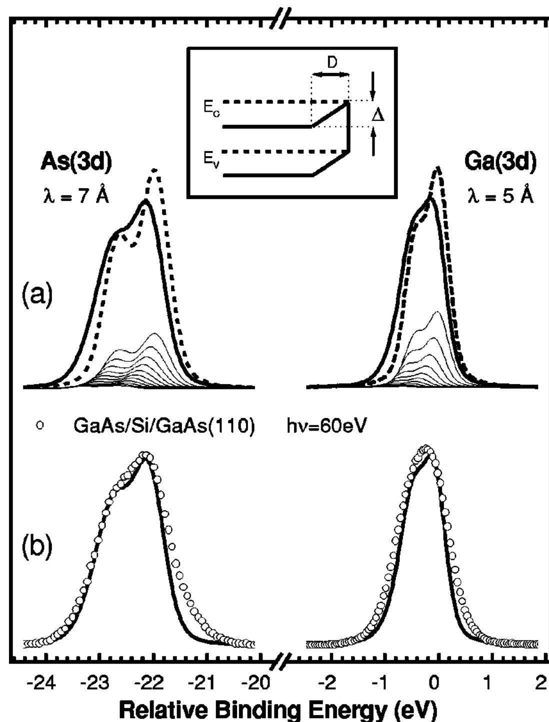

FIG. 8. (a) Modification of the shape of the As(3d) and Ga(3d) bulk components as a result of a sharp overlayer band bending. The dashed lines correspond to the emissions in an overlayer-flat-band configuration (represented as dashed in the inset), and have been taken directly from Fig. 6(a) [dotted line in Fig. 6(a)]. The thick solid lines correspond to the emissions calculated for the overlayer band-bent configuration (represented by solid lines in the inset: $D=20$ Å, $\Delta=0.7$ eV). The thick solid lines are the sum of the different monolayer contributions (thin solid lines), which are attenuated because of electron scattering, and shifted due to band bending. (b) Comparison of the bulk components calculated for the band-bent configuration (solid lines) with the experimental data obtained for GaAs/Si/GaAs(110) structures (open symbols).

ported in the literature have been used in the simulation.[51] The As(3d) and Ga(3d) line shapes calculated for the bulk emissions in the overlayer *band-bent* configuration are observed to be broader and shifted toward higher binding energies in relation to the line shapes corresponding to flatband conditions [Fig. 8(a)]. The former are compared in Fig. 8(b) with the spectra recorded on GaAs/Si/GaAs(110) (open symbols). The calculated peaks partially reproduce the experimental data. Although additional broadenings and the introduction of extra shifted components are required to fit the data completely, one may notice how the line shapes calculated for the bulk emissions lie well within the experimental spectra. Therefore, the existence of some kind of band-bending effect in our samples cannot be ruled out.

In summary, our results indicate that upon Si insertion at GaAs/GaAs(110) homojunctions, the Fermi level approaches the valence-band maximum at the surface. Some kind of chemical and/or structural disorder is also well evidenced. A Si-induced feature contributes to the As(3d) core-level emission in its low-binding-energy side. Effects such as: (i) a band-offset induction, or (ii) the occurrence of a sharp overlayer band bending, are both compatible with our data, although there is no direct evidence of either. Similarly to what was discussed in Sec. III A, a band-offset induction in a nonpolar GaAs/GaAs(110) homojunction would be difficult to understand within the ''interface microscopic capacitor'' picture, although it could be explained within a model based on the establishment of ''neutral nonequivalent interfaces.'' The apparent similarities between the raw data shown here for (110) homojunctions, and those previously reported for the (100) orientation, are well understood within a ''band-bending'' interpretation, since this effect is not critically dependent on the particular interface geometry.

IV. CONCLUSIONS

Synchrotron radiation photoemission results on the effect of submonolayer Si insertion at GaAs-on-AlAs(110) and GaAs/GaAs(110) nonpolar junctions have been reported. They have been compared with the results obtained on GaAs-on-AlAs(100) polar heterojunctions. The behavior of nonpolar (110) junctions has been found to be very similar to the one exhibited by polar (100) structures. Therefore, the interpretation of the experimental results as band-offset changes, based on the ''interface microscopic capacitor'' model, seems incorrect. Instead, the results can be well understood within an overlayer band-bending interpretation, without considering band-offset changes.

ACKNOWLEDGMENTS

We thank Dr. W. Braun for the flexibility in the beamtime scheduling necessary to coordinate the synchrotron experiments with the MBE sample growth. We gratefully acknowledge H. P. Schönherr and P. Schützendübe for their expert MBE assistance, I. Gorbunova, J. Behrend, and M. Wassermeier for their help in the AFM characterization, and C. Rojas, F. Schneider, S.-A. Ding, and S. Barman for technical assistance during the synchrotron beam times. One of us (M. M.) acknowledges the financial aid from the Comunidad Autónoma de Madrid, and the hospitality extended to her during her visit to the Paul-Drude-Institut. This work was partially supported by the Spanish Dirección General de Investigación Científica y Técnica under Grant Nos. PB94-53 and PB94-1530. The work at BESSY I was supported by the EU Human Capital and Mobility Program under Contract No. CHGE-CT93-0027.

*Electronic address: mmoreno@icmm.csic.es

[1] H. Kroemer, J. Vac. Sci. Technol. B **11**, 1354 (1993).
[2] G. Margaritondo, J. Vac. Sci. Technol. B **11**, 1362 (1993).
[3] W. R. Frensley and H. Kroemer, Phys. Rev. B **16**, 2642 (1977).
[4] W. A. Harrison, J. Vac. Sci. Technol. **14**, 1016 (1977).
[5] R. S. Bauer and H. W. Sang, Jr., Surf. Sci. **132**, 479 (1983).
[6] J. Tersoff, Phys. Rev. B **30**, 4874 (1984).
[7] W. A. Harrison, J. Vac. Sci. Technol. B **3**, 1231 (1985).
[8] F. Flores and C. Tejedor, J. Phys. C **20**, 145 (1987).
[9] E. O. Kane, J. Vac. Sci. Technol. A **5**, 1493 (1987).
[10] C. G. Van de Walle and R. M. Martin, Phys. Rev. B **35**, 8154 (1987).
[11] C. Priester, G. Allan, and M. Lannoo, J. Vac. Sci. Technol. B **11**, 1638 (1993).

[12] A. Franciosi and C. G. Van de Walle, Surf. Sci. Rep. **25**, 1 (1996).

[13] S. Baroni, R. Resta, A. Baldereschi, and M. Peressi, in *Spectroscopy of Semiconductor Microstructures,* Vol. 206 of *NATO Advanced Study Institute, Series B: Physics*, edited by G. Fasol, A. Fasolino, and P. Lugli (Plenum, London, 1989), p. 251.

[14] A. Baldereschi, R. Resta, M. Peresssi, S. Baroni, and K. Mäder, in *Semiconductor Interfaces at the Sub-Nanometer Scale,* Vol. 243 of *NATO Advanced Study Institute, Series E: Applied Sciences*, edited by H. W. M. Salemink and M.D. Pashley (Kluwer, Dordrecht, 1993), p. 59.

[15] C. G. Van de Walle and R. M. Martin, Phys. Rev. B **34**, 5621 (1986).

[16] C. G. Van de Walle and R. M. Martin, Phys. Rev. B **37**, 4801 (1988).

[17] W. R. L. Lambrecht and B. Segall, Phys. Rev. B **41**, 8353 (1990).

[18] R. G. Dandrea, C. B. Duke, and A. Zunger, J. Vac. Sci. Technol. B **10**, 1744 (1992).

[19] C. Weisbuch, J. Vac. Sci. Technol. A **12**, 1191 (1994).

[20] U. König, Phys. Scr. **T68**, 90 (1996).

[21] A. Muñoz, N. Chetty, and R. M. Martin, Phys. Rev. B **41**, 2976 (1990).

[22] M. Peressi, S. Baroni, R. Resta, and A. Baldereschi, Phys. Rev. B **43**, 7347 (1991).

[23] S. Baroni, R. Resta, and A. Baldereschi, in *Proceedings of the 19th International Conference on the Physics of Semiconductors,* edited by W. Zawadzki (Institute of Physics, Polish Academy of Sciences, Wroclaw, 1988), p. 525.

[24] L. Sorba, G. Bratina, G. Ceccone, A. Antonini, J. F. Walker, M. Micovic, and A. Franciosi, Phys. Rev. B **43**, 2450 (1991).

[25] M. Marsi, R. Houdre, A. Rudra, M. Ilegems, F. Gozzo, C. Coluzza, and G. Margaritondo, Phys. Rev. B **47**, 6455 (1993).

[26] M. Akazawa, H. Hasegawa, H. Tomazawa, and H. Fujikura, Jpn. J. Appl. Phys. **31**, L1012 (1992).

[27] Y. Hashimoto, G. Tanaka, and T. Ikoma, J. Vac. Sci. Technol. B **12**, 125 (1994).

[28] N. E. Christensen and L. Brey, Phys. Rev. B **38**, 8185 (1988).

[29] A. Muñoz and P. Rodríguez-Hernández, Phys. Rev. B **45**, 4502 (1992).

[30] W. I. Wang, J. Vac. Sci. Technol. B **1**, 630 (1983).

[31] L. T. P. Allen, E. R. Weber, J. Washburn, Y. C. Pao, and A. G. Elliot, J. Cryst. Growth **87**, 193 (1988).

[32] L. T. P. Allen, E. R. Weber, J. Washburn, and Y. C. Pao, Appl. Phys. Lett. **51**, 670 (1987).

[33] J. H. Neave, J. Zhang, X. M. Zhang, P. N. Fawcett, and B. A. Joyce, Appl. Phys. Lett. **62**, 753 (1993).

[34] M. Wassermeier, H. Yang, E. Tournié, L. Däweritz, and K. Ploog, J. Vac. Sci. Technol. B **12**, 2574 (1994).

[35] H. Yang, M. Wassermeier, E. Tournié, L. Däweritz, and K. Ploog, Surf. Sci. **331-333**, 479 (1995).

[36] K. H. Ploog and L. Däweritz, Jpn. J. Appl. Phys. **34**, 691 (1995).

[37] E. A. Kraut, R. W. Grant, J. R. Waldrop, and S. P. Kowalczyuk, Phys. Rev. Lett. **44**, 1620 (1980).

[38] R. W. Grant, E. A. Kraut, S. P. Kowalczyk, and J. R. Waldrop, J. Vac. Sci. Technol. B **1**, 320 (1983).

[39] E. A. Kraut, R. W. Grant, J. R. Waldrop, and S. P. Kowalczyk, Phys. Rev. B **28**, 1965 (1983).

[40] D. M. Bylander and L. Kleinman, Phys. Rev. B **41**, 3509 (1990).

[41] W. A. Harrison, E. A. Kraut, J. R. Waldrop, and R. W. Grant, Phys. Rev. B **18**, 4402 (1978).

[42] R. M. Martin, J. Vac. Sci. Technol. **17**, 978 (1980).

[43] R. G. Dandrea, S. Froyen, and A. Zunger, Phys. Rev. B **42**, 3213 (1990).

[44] G. Biasiol, L. Sorba, G. Bratina, R. Nicolini, A. Franciosi, M. Peressi, S. Baroni, R. Resta, and A. Baldereschi, Phys. Rev. Lett. **69**, 1283 (1992).

[45] D. E. Eastman, T.-C. Chiang, P. Heimann, and F. J. Himpsel, Phys. Rev. Lett. **45**, 656 (1980).

[46] T. Miller and T.-C. Chiang, Phys. Rev. B **29**, 7034 (1984).

[47] A. D. Katnani, H. W. Sang, Jr., P. Chiaradia, and R. S. Bauer, J. Vac. Sci. Technol. B **3**, 608 (1985).

[48] G. Le Lay, D. Mao, A. Kahn, Y. Hwu, and G. Margaritondo, Phys. Rev. B **43**, 14 301 (1991).

[49] R. Cimino, A. Giarante, K. Horn, and M. Pedio, Surf. Sci. **331-333**, 534 (1995).

[50] R. Cimino, A. Giarante, K. Horn, and M. Pedio, J. Electron Spectrosc. Relat. Phenom. **76**, 477 (1995).

[51] M. C. Schabel, I. M. Vitomirov, G. D. Waddill, and J. H. Weaver, J. Electron Spectrosc. Relat. Phenom. **56**, 211 (1991).